Tobias Bollhorst, Shakiba Shahabi, Katharina Wörz, Charlotte Petters, Prof. Ralf Dringen, Dr. Michael Maas, Prof. Kurosch Rezwan

Bifunctional Submicron Colloidosomes Coassembled from Fluorescent and Superparamagnetic Nanoparticles

Journal Article as: peer-reviewed accepted version (Postprint)

DOI of this document*(secondary publication): 10.26092/elib/2443

Publication date of this document: 16/09/2023

* for better findability or for reliable citation

Recommended Citation (primary publication/Version of Record) incl. DOI:

Bollhorst, T., Shahabi, S., Wörz, K., Petters, C., Dringen, R., Maas, M. and Rezwan, K. (2015), Bifunctional Submicron Colloidosomes Coassembled from Fluorescent and Superparamagnetic Nanoparticles. Angew. Chem. Int. Ed., 54: 118-123. https://doi.org/10.1002/anie.201408515

DOI: 10.1002/anie.201408515

Bifunctional Submicron Colloidosomes Coassembled from Fluorescent and Superparamagnetic Nanoparticles**

Tobias Bollhorst, Shakiba Shahabi, Katharina Wörz, Charlotte Petters, Ralf Dringen, Michael Maas, and Kurosch Rezwan*

Abstract: *Colloidosomes are microcapsules consisting of nanoparticle shells. These microcarriers can be self-assembled from a wide range of colloidal particles with selective chemical, physical, and morphological properties and show promise for application in the field of theranostic nanomedicine. Previous studies have mainly focused on fairly large colloidosomes (>1 μm) based on a single kind of particle; however, the intrinsic building-block nature of this microcarrier has not been exploited so far for the introduction of tailored functionality at the nanoscale. We report a synthetic route based on interfacial shear rheology studies that allows the simultaneous incorporation of different nanoparticles with distinct physical properties, that is, superparamagnetic iron oxide and fluorescent silica nanoparticles, in a single submicron colloidosome. These tailor-made microcapsules can potentially be used in various biomedical applications, including magnetic hyperthermia, magnetic particle imaging, drug targeting, and bioimaging.*

The controlled integration of multiple distinct physical properties into tailor-made vehicles is highly desirable for the improvement of various biomedical applications.[1–3] In particular, microcarrier systems have been investigated for their potential to improve cures for malignant tumors. A significant number of carriers are currently under development or have already made it from bench to bedside, including stealth liposomes,[4,5] mesoporous silica,[6,7] and polymeric nanoparticles.[8,9] Specifically for the targeted treatment of tumors, carriers should have submicron sizes so that the enhanced permeability and retention effect (EPR) can be exploited. The EPR effect is based on the passive accumulation of submicron particles around leaky tumor vasculature in combination with the impaired lymphatic drainage of submicron particles.[10] Carriers should ideally be synthesized in a size range smaller than 1 μm and greater than 8 nm, first to make use of the EPR effect, and second to prevent diffusion into healthy tissue, since particles featuring diameters which are too small (≤8 nm)[11] might lose their selectivity for cancerous tumors. Recent studies have further shown that hierarchical carrier systems that can disassemble when they reach a tumor site enable deeper penetration of the individual building blocks into malignant tissue.[12,13] Nanoparticle-based treatment and imaging methods, such as magnetic hyperthermia as well as magnetic and fluorescence bioimaging, would be beneficial to improve the diagnosis and cure of various types of tumors. Thus, hierarchically assembled capsules of submicron size with tailorable physical properties are highly promising for drug delivery and theranostics.

Colloidosomes are a rapidly emerging class of microcarriers that possess great potential for the design of capsules with the aforementioned properties. This type of microcapsule features a nanoporous shell formed from colloidal particles and a liquid core for potential drug encapsulation.[14] Previous studies have mainly focused on microsized (>1 μm) colloidosomes based on a single kind of particle with one distinct physical or morphological characteristic, such as iron oxide particles,[15,16] polymeric microrods,[17] and cubic metal–organic frameworks.[18] Initial studies have also been performed on multiwalled colloidosomes,[19] colloidosomes doped with a single variable nanoparticle,[20] colloidosomes for enzyme encapsulation,[21,22] colloidosome-based drug carriers,[23] and inorganic colloidosomes for the investigation of artificial cells (protocells).[24] However, the intrinsic building-block nature of this microcarrier has not been exploited so far for the introduction of tailored functionality at the nanoscale.

In this study, we addressed this challenge by coassembling superparamagnetic iron oxide nanoparticles (SPIONs) and fluorescent-dye-doped silica nanoparticles (FSNPs) into submicron colloidosomes. SPIONs and FSNPs are two particle types that are of special interest for coassembly into hollow capsules. Their specific physical characteristics can potentially be utilized for combined treatment and diagnostic methods; that is, magnetic fluid hyperthermia (MFH),[25] magnetic particle imaging (MPI),[26] on-site biosensing,[27] bioimaging, and tracing of the cellular uptake of nanoparticles.[28] The assembly of submicron colloidosomes was recently established and demonstrated by our group with either metal-oxide nanoparticles[29] or nanodiamonds[30] as building blocks, in

[*] T. Bollhorst, S. Shahabi, K. Wörz, Dr. M. Maas, Prof. K. Rezwan
Department of Production Engineering, Advanced Ceramics
University of Bremen
Am Biologischen Garten 2, Bremen (Germany)
E-mail: michael.maas@uni-bremen.de
C. Petters, Prof. R. Dringen
Centre for Biomolecular Interactions Bremen and
Center for Environmental Research and Sustainable Technology
University of Bremen
Leobener Strasse, Bremen (Germany)

[**] We are grateful for funding by the German Research Foundation (DFG) by the grant MA4795/5-1, for support within the DFG research training group 1860 "Micro-, Meso-, and Macroporous Nonmetallic Materials: Fundamentals and Applications" (MIMENIMA), and for funding by the European Union nanomaterials safety testing infrastructure QualityNano (INFRA-2010-1.1.31).
Supporting information for this article is available on the WWW under http://dx.doi.org/10.1002/anie.201408515.

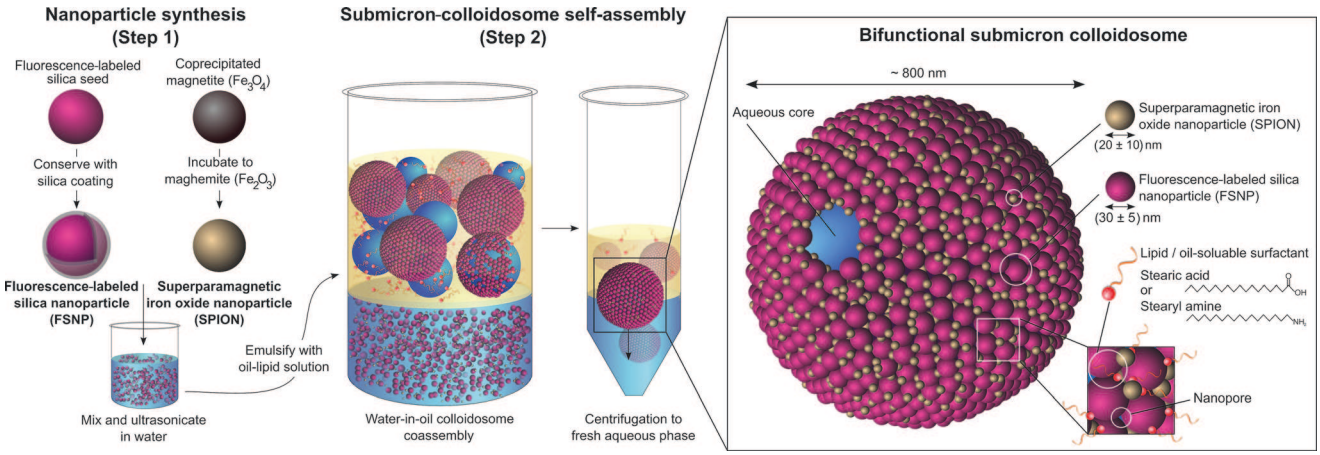

Figure 1. Schematic illustration of the synthetic route based on self-assembly and properties of a nanoporous bifunctional submicron colloidosome. Step 1: Fluorescence-labeled silica nanoparticles were synthesized by the regrowth of silica seeds tagged with rhodamine B isothiocyanate; superparamagnetic iron oxide nanoparticles were prepared by classical coprecipitation of Fe^{2+} and Fe^{3+} ions and were thoroughly cleaned by dialysis. Step 2: Bifunctional submicron colloidosomes were coassembled at the interface of emulsion droplets in a water-in-decane miniemulsion with self-assembly-inducing lipids dissolved in the decane phase; the capsules were finally transferred to a fresh aqueous phase. The self-assembled colloidosomes feature bifunctionality in the form of fluorescence and superparamagnetism and could potentially enable the encapsulation and release of active agents from the aqueous core.

combination with oil-soluble surfactants. Because of their negligible solubility in water along with their derivation from fats, we refer to these surfactants as lipids. Prior to colloidosome synthesis, the shell-forming colloidal particles are synthesized and dispersed in an aqueous medium (Figure 1, step 1). Afterwards, submicron colloidosomes are synthesized by generating a water-in-oil miniemulsion, in which the nanoparticles then self-assemble at the emulsion-droplet interfaces (Figure 1, step 2). Submicron colloidosome formation is most successfully carried out with nanoparticles and lipids of the same net charge, which form a thin film at the emulsion-droplet fluid–fluid interface. As detailed previously,[29,31] the formation of rigid interfacial particle films is probably caused by interactions of the lipid molecules with the nanoparticles at the interface. The oil–water interface of the emulsion droplets is populated by a Gibbs adsorption layer of the surface-active lipid molecules. When the nanoparticles adsorb at the oil–water interface, the surface-charge interactions between the particles are mitigated by the lipid molecules, which act as a local electrolyte. As a result, nanoparticles accumulate at the droplet interfaces and undergo controlled self-assembly. The intrinsically rigid capsules are subsequently transferred to a fresh aqueous phase.

The synthesis is performed at near-neutral pH and ambient temperature and yields spherical capsules with diameters below 1 μm, as required for biomedical applications. For the synthesis of colloidosomes with submicron diameters, the emulsion droplets, which act as the size and shape template of the colloidosomes, are formed by strong ultrasonication in a water bath. The process for the formation of the interfacial films, which form the colloidosome shell on aqueous emulsion droplets, can be controlled by lipids that bear a charge of the same sign as that of the colloidosome-forming particles.[29,31] Either a positively charged lipid is used with likewise positively charged nanoparticles or a negatively charged lipid is used with particles exhibiting a negative ζ potential. However, as we now report, the addition of a small amount of oppositely charged nanoparticles also leads to successful capsule formation, thus enabling the assembly of bifunctional colloidosomes.

Prior to colloidosome self-assembly, the microcapsule-forming SPION and FSNP building blocks were synthesized. SPIONs (Figure 2a, left) were obtained by the coprecipitation of Fe^{2+} and Fe^{3+} ions under alkaline conditions, thus resulting in the formation of a stable superparamagnetic liquid (see Figure S1 in the Supporting Information).[32] To decrease the free-ion concentration of the SPION liquid, we exchanged the dispersing medium by dialysis, thus shifting the pH value to a less acidic value of 5.5. This step is important, as otherwise a high residual amount of free ions from the initial synthesis would strongly hamper colloidosome formation (see Figure S2). The synthesis of photostable and monodisperse fluorescently labeled silica nanoparticles (Figure 2b, left) is based on a silica-seed-regrowth process.[33,34] Silica seeds were tagged with rhodamine B isothiocyanate (RBITC), and a thin silica layer was then added to conserve and protect the fluorescent marker from future degradation (see the Supporting Information for the detailed synthetic route.)

Before these two particle types were combined in a single capsule, colloidosomes were synthesized with the respective SPION and FSNP particles individually (see Figures S3 and S4). Decane was chosen for the oil phase, as it can be purchased in very high purity. The lipid stearic acid (pK_a 4.9) or stearyl amine (pK_a 10.6) was used in the procedure. During the emulsification process, the lipid molecules dissociate their hydrophilic head group at the emulsion-droplet interface and complement the self-assembly of SPIONs or FSNPs at the liquid–liquid emulsion-droplet interface (Figure 1, magnification).

The morphology of colloidosomes with closed and open shells (Figure 2a,b, middle images) was visualized by scanning

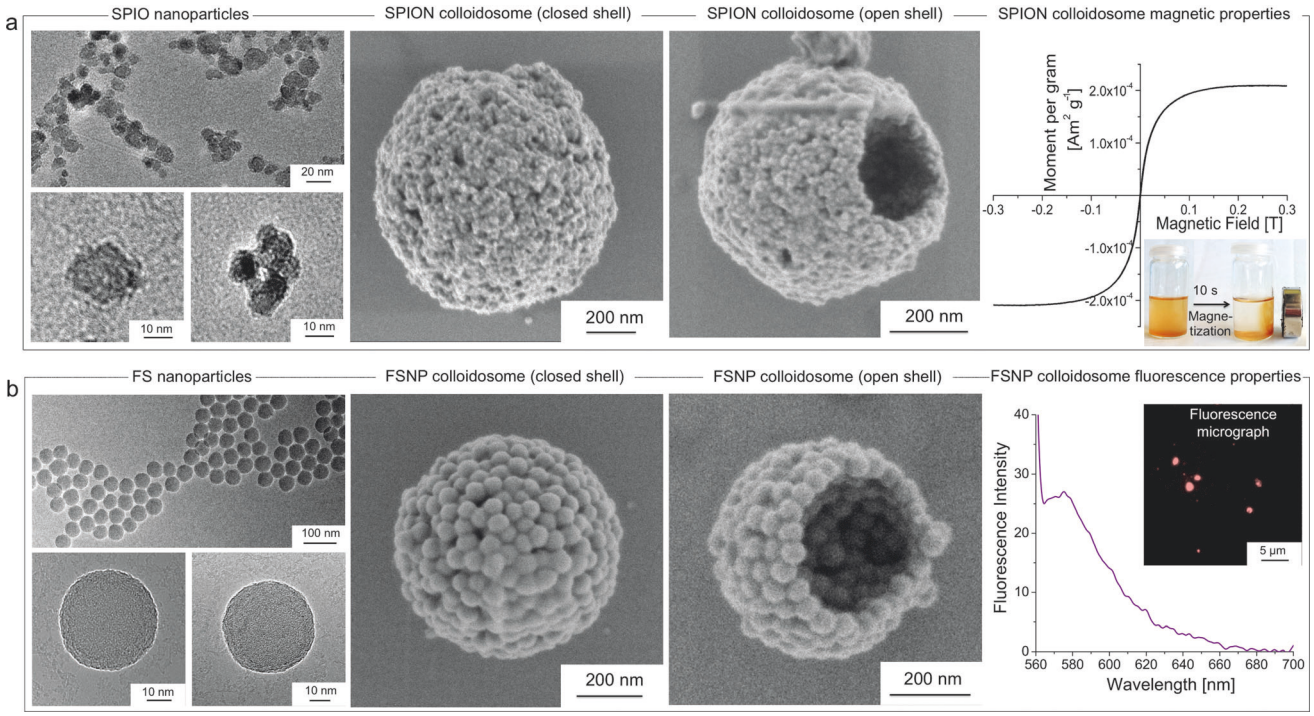

Figure 2. Left: TEM micrographs of the prepared functional a) SPIO and b) FS nanoparticles. The SPIONs have an average diameter of around (20±10) nm and show some aggregates/agglomerates. FSNPs show very high uniformity and have a diameter of (30±5) nm. Center images: SEM micrographs of submicron colloidosomes with closed shells and open-shelled colloidosomes. The latter images reveal the hollow interior of some colloidosomes. a) The superparamagnetic colloidosomes possess a thin multilayer of SPIONs in the shell, whereas b) the fluorescent colloidosomes solely feature a single layer of FSNPs. Right: a) SPION colloidosomes show ideal superparamagnetic functionality with neither remanence magnetization nor a coercive field force (inset shows the high responsiveness of SPION colloidosomes to an external magnetic field). b) FSNP colloidosomes feature high fluorescence intensity (inset shows a fluorescence microscope image).

electron microscopy (SEM). SPION colloidosomes were synthesized with stearyl amine (see Figure S3) and exhibited no discernable surface order, whereas the FSNP colloidosomes, formed with stearic acid (see Figure S4), featured a roughly hexagonal close-packed surface structure. SEM micrographs of colloidosomes with open shells revealed the hollow interior of some structures (Figure 2); the superparamagnetic colloidosomes possessed a thin multilayer of SPIONs in the shell, whereas the fluorescent colloidosomes featured only a single layer of FSNPs. The SPION colloidosomes exhibited ideal superparamagnetic properties without remanence magnetization or a coercive field force, as revealed by the hysteresis loop generated with a magnetometer (Figure 2a, right). Thus, these microcapsules are an ideal candidate for MFH and MPI. The high fluorescence intensity of the FSNPs enabled direct observation with a fluorescence microscope (Figure 2b, right). Thus, this colloidosome type could potentially be used for bioimaging applications. In preliminary studies, the submicron colloidosomes were further shown to feature mechanical stability in centrifugation tests, while also possessing adequate stability in buffers and blood serum.

To elucidate the process of colloidosome formation, we used a double-wall-ring (DWR) setup in combination with interfacial shear rheology (ISR; Figure 3a).[35] Colloidosome formation can be interpreted as the growth of ultrathin films of nanoparticles and lipid molecules at the fluid–fluid interface of water-in-oil-emulsion droplets.[31] This thin-film growth process is similar to the formation of (Ramsden)–Pickering emulsions, in which particles adsorb between two immiscible liquids and stabilize the emulsion droplet against coalescence or Ostwald ripening by forming a particle monolayer at the emulsion-droplet interface.[36,37] In our study, the three-dimensional curved interface of emulsion water droplets in the oil phase was transferred to a two-dimensional planar interface (Figure 3a, bottom). For the ISR setup, a metal ring (Pt/Ir Du Noüy ring)[35,38] is directly positioned at the interface between the water phase containing colloidal particles and the oil phase containing lipid molecules. Over time, an increasing number of lipid molecules accumulate at the oil–water interface, where the functional head groups of the lipids dissociate. We think that the resulting charge induction at the interface interferes with the electrical double layer of colloidal particles in close proximity to the interface, thus promoting their accumulation at the interface and leading to the corresponding thin-film growth. This process can be controlled by the correct choice of lipid type and concentration; direct correlations can be made, thus enabling the optimization of conditions for successful colloidosome formation (see the Supporting Information for detailed experimental conditions).

After the application of a sinusoidal oscillation on the Du Noüy ring, we measured the resultant shear deformation of the interfacial film to analyze the formation of the

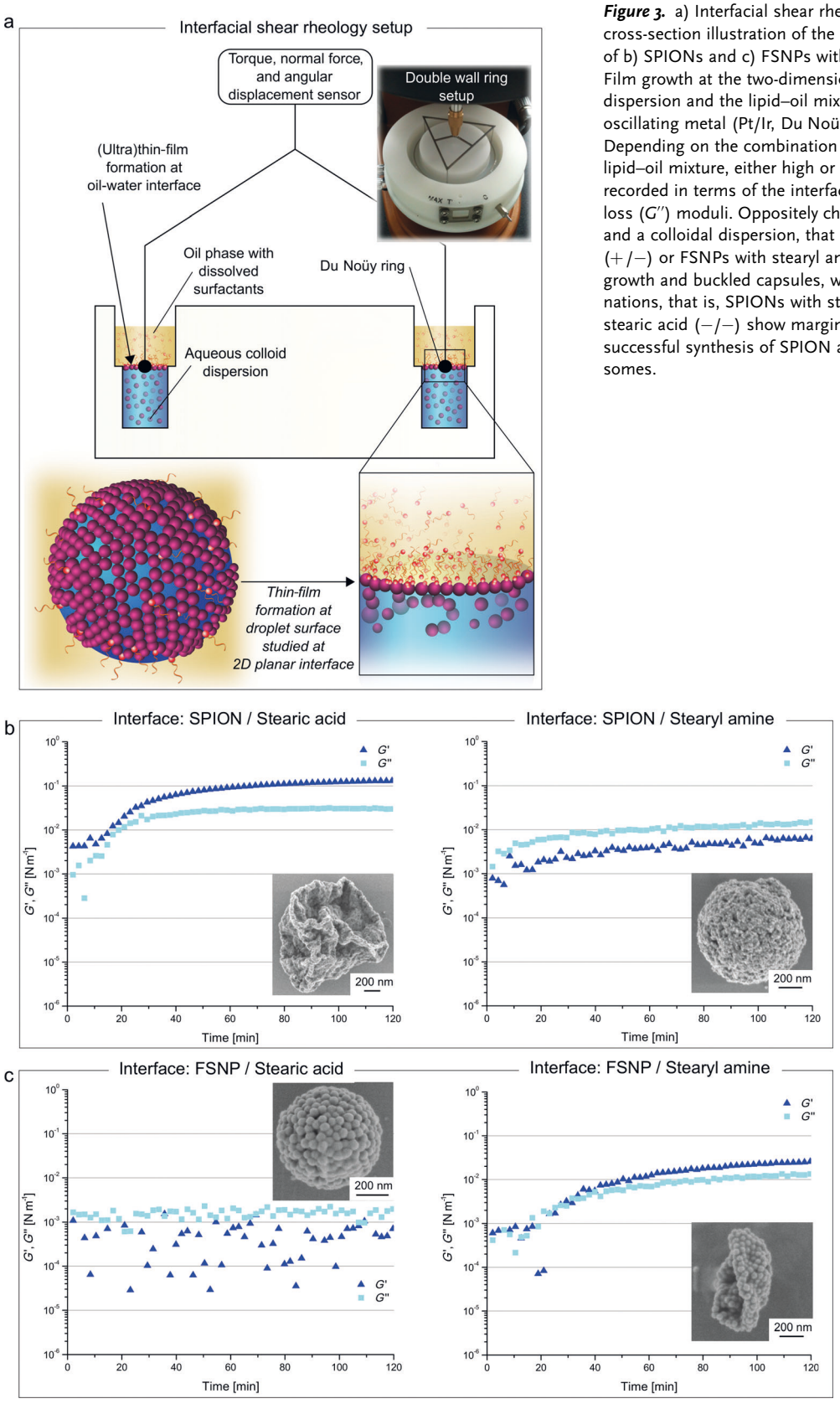

Figure 3. a) Interfacial shear rheology setup with a schematic cross-section illustration of the setup, and results for dispersions of b) SPIONs and c) FSNPs with stearic acid and stearyl amine. Film growth at the two-dimensional interface between the colloid dispersion and the lipid–oil mixture is determined by placing an oscillating metal (Pt/Ir, Du Noüy) ring directly at the interface. Depending on the combination of the colloidal dispersion and the lipid–oil mixture, either high or only marginal film growth may be recorded in terms of the interfacial rheological storage (G') and loss (G'') moduli. Oppositely charged combinations of a surfactant and a colloidal dispersion, that is, SPIONs with stearic acid (+/−) or FSNPs with stearyl amine (−/+), lead to strong film growth and buckled capsules, whereas identically charged combinations, that is, SPIONs with stearyl amine (+/+) or FSNPs with stearic acid (−/−) show marginal film growth and enable the successful synthesis of SPION and FSNP submicron colloidosomes.

nanoparticle–lipid film in terms of the interfacial shear storage (G') and loss (G'') moduli. Figure 3b shows the increase in G' and G'' of positively charged SPION particles at the oil–water interface over time in comparison to either the negatively charged lipid stearic acid or the positively charged lipid stearyl amine. The results show higher interfacial shear moduli for the combination of positively charged SPIONs with stearic acid than with stearyl amine. SEM micrographs of colloidosomes formed with the same particle/lipid composition directly revealed that SPION capsules formed with stearyl amine were spherical and intrinsically stable (Figure 3b, right, inset), whereas those synthesized with stearic acid existed as large agglomerates and deflated capsule-like structures featuring folds and creases (Figure 3b, left, inset). The formation of deflated structures with stearic acid is most likely caused by strong and nonspecific aggregation of the oppositely charged lipids and particles; this behavior apparently also leads to a buckling of the capsules right after their formation during the ultrasonication step or later during the drying process. Similar observations were made for the negatively charged FSNPs (Figure 3c): We

found that a combination of identically charged surfactants (stearic acid) and nanoparticles led to ideal colloidosome formation (Figure 3c, insets). In general, our interfacial rheology findings clearly indicate that identically charged lipid/colloid combinations lead to the formation of ultrathin films and allow successful and controlled colloidosome self-assembly, whereas oppositely charged combinations lead to disproportionate film formation, which results in large aggregates as well as "deflated" and irregular colloidosomes.

On the basis of the interfacial shear rheology findings, we examined the coassembly of bifunctional colloidosomes. In this case, FSNPs were dispersed by ultrasonication in dialyzed water containing a low amount of SPIONs, and then the synthesis of bifunctional colloidosomes was carried out in a 1 mM solution of stearic acid in decane. In an extensive study, we found that the ideal ratio of FSNPs to SPIONs in the initial colloidal dispersion for the formation of a mixed colloidosome shell was 10:1 (1 vol% FSNPs, 0.1 vol% SPIONs). After coassembly, the smaller SPIONs were well-integrated between the FSNPs in the capsule shell (Figure 4, top left). The high element-specific contrast of energy-selective backscatter (EsB)[39,40] scanning electron microscopy (Figure 4, top right) further showed the nanoscale composition of the novel hybrid colloidosome. A pseudo color image prepared on the basis of the EsB micrograph illustrates the combined integration of SPIONs and FSNPs more clearly (Figure 4, bottom left). Similar to the colloidosomes prepared from the individual particles, the bifunctional submicron colloidosome exhibited simultaneous superparamagnetic and fluorescence bifunctionality (Figure 4, bottom right). Other SPION/FSNP ratios with varying surfactant concentrations still led to the formation of colloidosomes containing both particles types (see Figure S5a for additional micrographs showing simultaneous SPION and FSNP incorporation); however, in most cases we observed either a less ideal particle mixing in the colloidosome shell (see Figure S5b) or "deflated" structures (see Figure S5c). Furthermore, a possible fluorescence-quenching effect can be neglected, as we only observed a decrease in the fluorescence intensity for very high SPION concentrations (see Figure S6).

The approach of utilizing both superparamagnetic and fluorescent particles in a single colloidosome is the first step toward creating a novel design tool for the synthesis of nanotheranostic vehicles. Instead of SPIONs or FSNPs, entirely different particles exhibiting other distinct properties may be used additionally or as substitutes in the microcapsule shell, such as gold nanoparticles, quantum dots, calcium carbonate particles, nanodiamonds, and drug-loaded particles. In future studies, bifunctional submicron colloidosomes may be utilized for the incorporation of a broad range of cytostatic agents in combination with an increase in biocompatibility. Furthermore, submicron colloidosomes may be surface-functionalized to increase their circulation time in the blood stream, in analogy with stealth nanoparticles. Additionally,

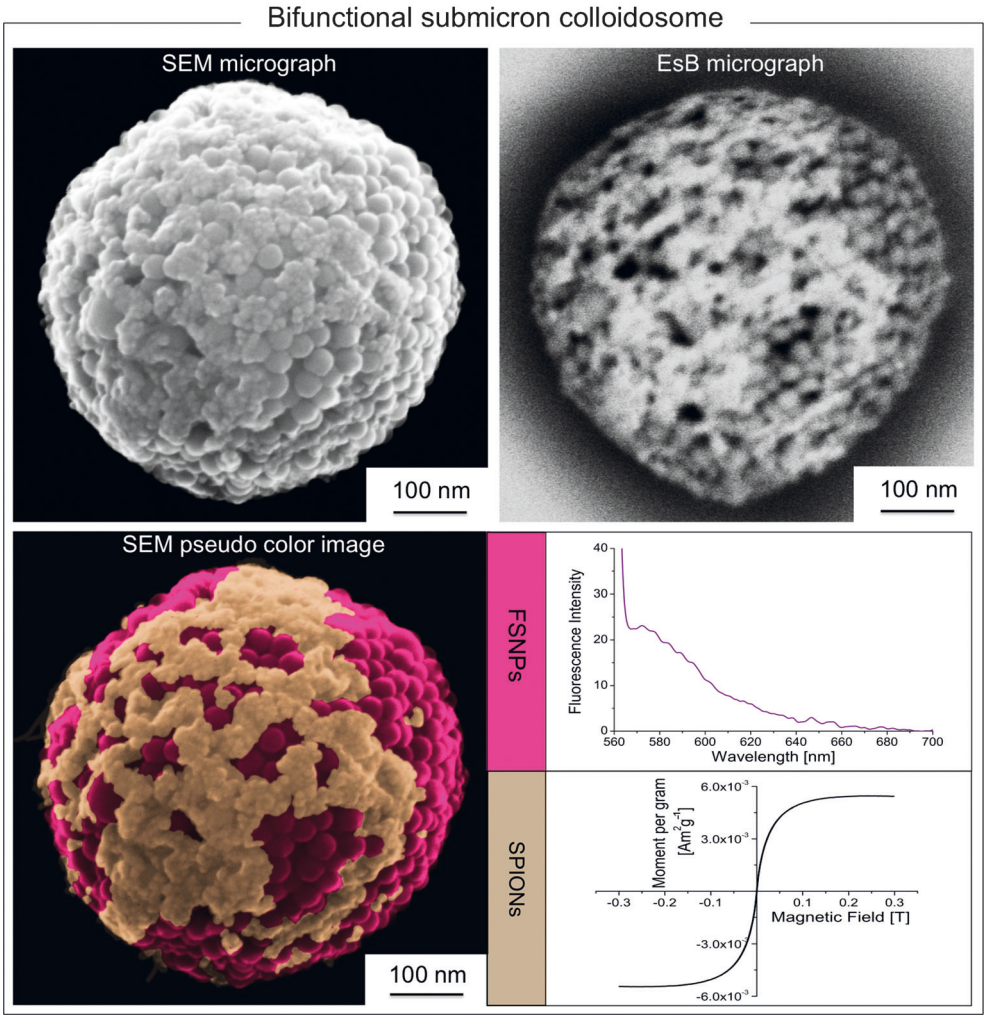

Figure 4. Top left: SEM micrograph of a bifunctional superparamagnetic/fluorescent submicron colloidosome showing coassembled SPIONs (small particles) and FSNPs (large particles). Top right: Energy-selective backscatter SEM micrograph enabling the visual nanoscale differentiation of SPIONs (bright particles) and FSNPs (darker particles). Bottom left: SEM pseudo color image illustrating the distribution of FSNPs and SPIONs within the colloidosome shell. Bottom right: Distinct fluorescence and superparamagnetic properties of the bifunctional colloidosome containing both FSNPs and SPIONs.

the interactions of colloidosomes in physiological solutions and their suitability for biomedical applications, including drug delivery to tumor cells, hyperthermia treatment of cancer, and visualization of the localization of colloidosomes both in cells by fluorescence microscopy as well as in tissues by magnetic particle imaging (MPI), may be investigated.

In summary, the ability to create capsules with a membrane shell composed of SPIONs and FSNPs as well as potential further types of nanoparticles allows the tailor-made design of microcarriers with nanoparticle shells. We were able to show that it is possible to incorporate nanoparticles with distinct physical properties into the shell of submicron colloidosomes. The formation process of SPION and FSNP capsules was studied by interfacial shear rheology, which allowed a direct correlation for successful colloidosome formation. The ability to incorporate selective physical properties on the nanoscale into a submicron capsule might prove highly beneficial for targeted drug delivery and theranostic applications.

Received: August 25, 2014
Revised: October 6, 2014
Published online: November 4, 2014

Keywords: colloidosomes · fluorescence · interfacial shear rheology · superparamagnetism · theranostics

[1] B. P. Barnett, A. Arepally, M. Stuber, D. R. Arifin, D. L. Kraitchman, J. W. M. Bulte, *Nat. Protoc.* **2011**, *6*, 1142 – 1151.
[2] G. von Maltzahn, J.-H. Park, K. Y. Lin, N. Singh, C. Schwöppe, R. Mesters, W. E. Berdel, E. Ruoslahti, M. J. Sailor, S. N. Bhatia, *Nat. Mater.* **2011**, *10*, 545 – 552.
[3] J. Guo, Y. Ping, H. Ejima, K. Alt, M. Meissner, J. J. Richardson, Y. Yan, K. Peter, D. von Elverfeldt, C. E. Hagemeyer, et al., *Angew. Chem. Int. Ed.* **2014**, *53*, 5546 – 5551; *Angew. Chem.* **2014**, *126*, 5652 – 5657.
[4] Y. (Chezy) Barenholz, *J. Controlled Release* **2012**, *160*, 117 – 134.
[5] V. Plassat, C. Wilhelm, V. Marsaud, C. Ménager, F. Gazeau, J.-M. Renoir, S. Lesieur, *Adv. Funct. Mater.* **2011**, *21*, 83 – 92.
[6] C. E. Ashley, E. C. Carnes, G. K. Phillips, D. Padilla, P. N. Durfee, P. A. Brown, T. N. Hanna, J. Liu, B. Phillips, M. B. Carter, N. J. Carroll, X. Jiang, D. R. Dunphy, C. L. Willman, D. N. Petsev, D. G. Evans, A. N. Parikh, B. Chackerian, W. Wharton, D. S. Peabody, C. J. Brinker, *Nat. Mater.* **2011**, *10*, 389 – 397.
[7] Z. Li, J. C. Barnes, A. Bosoy, J. F. Stoddart, J. I. Zink, *Chem. Soc. Rev.* **2012**, *41*, 2590 – 2605.
[8] L. Liao, J. Liu, E. C. Dreaden, S. W. Morton, K. E. Shopsowitz, P. T. Hammond, J. A. Johnson, *J. Am. Chem. Soc.* **2014**, *136*, 5896 – 5899.
[9] E. Kim, D. Kim, H. Jung, J. Lee, S. Paul, N. Selvapalam, Y. Yang, N. Lim, C. G. Park, K. Kim, *Angew. Chem. Int. Ed.* **2010**, *49*, 4405 – 4408; *Angew. Chem.* **2010**, *122*, 4507 – 4510.
[10] E. K.-H. Chow, D. Ho, *Sci. Transl. Med.* **2013**, *5*, 216rv4 – 216rv4.
[11] M. E. Fox, F. C. Szoka, J. M. J. Fréchet, *Acc. Chem. Res.* **2009**, *42*, 1141 – 1151.
[12] C. Ju, R. Mo, J. Xue, L. Zhang, Z. Zhao, L. Xue, Q. Ping, C. Zhang, *Angew. Chem. Int. Ed.* **2014**, *53*, 6253 – 6258; *Angew. Chem.* **2014**, *126*, 6367 – 6372.
[13] C. Wong, T. Stylianopoulos, J. Cui, J. Martin, V. P. Chauhan, W. Jiang, Z. Popović, R. K. Jain, M. G. Bawendi, D. Fukumura, *Proc. Natl. Acad. Sci. USA* **2011**, *108*, 2426 – 2431.
[14] A. D. Dinsmore, M. F. Hsu, M. G. Nikolaides, M. Marquez, A. R. Bausch, D. A. Weitz, *Science* **2002**, *298*, 1006 – 1009.
[15] H. Duan, D. Wang, N. S. Sobal, M. Giersig, D. G. Kurth, H. Möhwald, *Nano Lett.* **2005**, *5*, 949 – 952.
[16] B. Samanta, D. Patra, C. Subramani, Y. Ofir, G. Yesilbag, A. Sanyal, V. M. Rotello, *Small* **2009**, *5*, 685 – 688.
[17] P. F. Noble, O. J. Cayre, R. G. Alargova, O. D. Velev, V. N. Paunov, *J. Am. Chem. Soc.* **2004**, *126*, 8092 – 8093.
[18] M. Pang, A. J. Cairns, Y. Liu, Y. Belmabkhout, H. C. Zeng, M. Eddaoudi, *J. Am. Chem. Soc.* **2013**, *135*, 10234 – 10237.
[19] J. S. Sander, A. R. Studart, *Soft Matter* **2014**, *10*, 60.
[20] X.-W. Xu, X.-M. Zhang, C. Liu, Y.-L. Yang, J.-W. Liu, H.-P. Cong, C.-H. Dong, X.-F. Ren, S.-H. Yu, *J. Am. Chem. Soc.* **2013**, *135*, 12928 – 12931.
[21] P. H. R. Keen, N. K. H. Slater, A. F. Routh, *Langmuir* **2014**, *30*, 1939 – 1948.
[22] C. Zhang, C. Hu, Y. Zhao, M. Möller, K. Yan, X. Zhu, *Langmuir* **2013**, *29*, 15457 – 15462.
[23] F. Porta, A. Kros, *Part. Part. Syst. Charact.* **2013**, *30*, 606 – 613.
[24] M. Li, R. L. Harbron, J. V. M. Weaver, B. P. Binks, S. Mann, *Nat. Chem.* **2013**, *5*, 529 – 536.
[25] M. Mahmoudi, S. Sant, B. Wang, S. Laurent, T. Sen, *Adv. Drug Delivery Rev.* **2011**, *63*, 24 – 46.
[26] B. Gleich, J. Weizenecker, *Nature* **2005**, *435*, 1214 – 1217.
[27] W. Park, M. J. Kim, Y. Choe, S. K. Kim, K. Woo, *J. Mater. Chem. B* **2014**, *2*, 1938 – 1944.
[28] S. W. Bae, W. Tan, J.-I. Hong, *Chem. Commun.* **2012**, *48*, 2270.
[29] T. Bollhorst, T. Grieb, A. Rosenauer, G. Fuller, M. Maas, K. Rezwan, *Chem. Mater.* **2013**, *25*, 3464 – 3471.
[30] M. Maas, T. Bollhorst, R. N. Zare, K. Rezwan, *Part. Part. Syst. Charact.* **2014**, *31*, 1067 – 1071.
[31] M. Maas, C. C. Ooi, G. G. Fuller, *Langmuir* **2010**, *26*, 17867 – 17873.
[32] M. Geppert, M. Hohnholt, L. Gaetjen, I. Grunwald, M. Bäumer, R. Dringen, *J. Biomed. Nanotechnol.* **2009**, *5*, 285 – 293.
[33] R. Watanabe, T. Yokoi, E. Kobayashi, Y. Otsuka, A. Shimojima, T. Okubo, T. Tatsumi, *J. Colloid Interface Sci.* **2011**, *360*, 1 – 7.
[34] K. D. Hartlen, A. P. T. Athanasopoulos, V. Kitaev, *Langmuir* **2008**, *24*, 1714 – 1720.
[35] S. Vandebril, A. Franck, G. G. Fuller, P. Moldenaers, J. Vermant, *Rheol. Acta* **2010**, *49*, 131 – 144.
[36] J. Krägel, S. R. Derkatch, *Curr. Opin. Colloid Interface Sci.* **2010**, *15*, 246 – 255.
[37] O. S. Deshmukh, D. van den Ende, M. Cohen Stuart, F. Mugele, M. H. G. Duits, *Adv. Colloid Interface Sci.*, DOI: 10.1016/j.cis.2014.09.003.
[38] G. G. Fuller, J. Vermant, *Annu. Rev. Chem. Biomol. Eng.* **2012**, *3*, 519 – 543.
[39] H. Jaksch, M. Steigerwald, V. Drexel, *Microsc. Microanal.* **2005**, *11*, 758 – 759.
[40] M. D. G. Steigerwald, R. Arnold, J. Bihr, V. Drexel, H. Jaksch, D. Preikszas, J. P. Vermeulen, *Microsc. Microanal.* **2004**, *10*, 1372 – 1373.